

Inner-Imaging Networks: Put Lenses into Convolutional Structure

Yang Hu, *Student Member, IEEE*, Guihua Wen, Mingnan Luo, Dan Dai, Wenming Cao, Zhiwen Yu, *Senior Member, IEEE*, and Wendy Hall

Abstract—Despite the tremendous success in computer vision, deep convolutional networks suffer from serious computation costs and redundancies. Although previous works address this issue by enhancing diversities of filters, they have not considered the complementarity and the completeness of the internal structure of the convolutional network. To deal with these problems, a novel Inner-Imaging architecture is proposed in this paper, which allows relationships between channels to meet the above requirement. Specifically, we organize the channel signal points in groups using convolutional kernels to model both the intra-group and inter-group relationships simultaneously. The convolutional filter is a powerful tool for modeling spatial relations and organizing grouped signals, so the proposed methods map the channel signals onto a pseudo-image, like putting a lens into convolution internal structure. Consequently, not only the diversity of channels is increased, but also the complementarity and completeness can be explicitly enhanced. The proposed architecture is lightweight and easy to be implemented. It provides an efficient self-organization strategy for convolutional networks so as to improve their efficiency and performance. Extensive experiments are conducted on multiple benchmark image recognition data sets including CIFAR, SVHN and ImageNet. Experimental results verify the effectiveness of the Inner-Imaging mechanism with the most popular convolutional networks as the backbones.

Index Terms—Convolutional networks, channel-wise attention, grouped relationships, inner-imaging.

I. INTRODUCTION

DEEP convolutional neural networks (CNNs) have exhibited significant effectiveness in modeling image data [1], [2], [3], [4], [5], [6], [7], their structures have also been constantly explored [8], [9], [10], [11], [12], [13]. Meanwhile, CNNs show the bulky size and serious redundancy [14], [15]. Besides pruning a complete structure [16], [17], [18], lots of methods aim to improve the efficiency of CNNs [19], [20]. Generally, the efficiency heavily depend on the interior components of CNNs which should meet the following requirements: diversity, complementarity and completeness. As the basic elements of CNNs, convolutional filters are often modeled to implement channel-wise attention [21], which only focuses on improving the diversity of feature maps, and lacks explicit modeling of complementarity and completeness of convolution channels.

Yang Hu, Guihua Wen (corresponding author), Mingnan Luo, Dan Dai, Zhiwen Yu are with the School of Computer Science and Engineering, South China University of Technology, China. Email: superhy199148@hotmail.com (first author), crghwen@scut.edu.cn (corresponding author), Phone no: +86-18998384808.

Wenming Cao is with the Department of Computer Science, City University of Hong Kong, Hong Kong. Email: wenmincao2-c@my.cityu.edu.hk.

Wendy Hall is with the Web Science Institute, University of Southampton, UK. Email: wh@ecs.soton.ac.uk, Phone no: +44(0)2380592388.

There are some methods have modeled and explored the grouping relationship between convolution channels [22], [23], [24]. Their excellent performances indicate that implicit group relations exist between convolutional feature maps. However, the grouping relations are ignored in the ordinary channel-wise attention methods. Since their plain fully connected (FC) encoder cannot represent the detailed grouping and interaction of channel relationships. In other words, these methods have not explicitly modeled the coordination and complementarity between channels.

In order to overcome the above shortcomings, this paper proposes a novel "Inner-Imaging" (InI) mechanism, as shown in Fig.1(b), which is a new way to model the channel relationships. Specifically, it first rearranges the feature signals into a pseudo-image $\hat{v} \in \mathbb{R}^{n \times m}$, then it creates grouping filters (G-filters) $w_{(n \times m)}$ to scan on it. In this process, channel signals $u_{ij} \in \hat{v}$ within a same receptive field can build relations from multiple directions (top, down, left, right, top left, top right, bottom left, bottom right, and so on), and are assigned into one group. Subsequently, InI adopts FC layers to model group-wise relationships. That is, the G-filters are responsible for modeling relations between channels which in the same group, the followed FC layers are used to model the relationships between groups. With this strategy, the complementarities of both convolutional channels and channel groups are enhanced. On the other hand, the size of channel groups can be flexibly controlled by adjusting the shape of G-filters (such as G-filters $w_{(1 \times 1)}$ with shape 1×1 representing the groups with the single channel). In this way, the completeness of representation of channels can be improved by integrating multi-scale G-filters. The InI-model provides a more complete and precise convolution channel relationship modeling method and provides the channels more rational re-scaling weights.

The exploration of CNN architecture and modeling of network internal representation is a meaningful and challenging task [25], [26], [27], [28]. The design of "Inner-Imaging" brings a new idea of convolution internal structure modeling. It also provides us a carrier to explore grouping modes of convolution channels. The InI architecture can be applied to all kinds of CNNs so as to improve the efficiency of CNNs, it is lightweight and easy to implement and understand.

Our contributions can be summarized as follows:

- A novel "Inner-Imaging" (InI) mechanism is proposed, which first uses G-filters to organize channel signals, and simultaneously models the intra-group channel relationships and the inter-group channel relationships. Some theoretical deductions of InI are also provided.

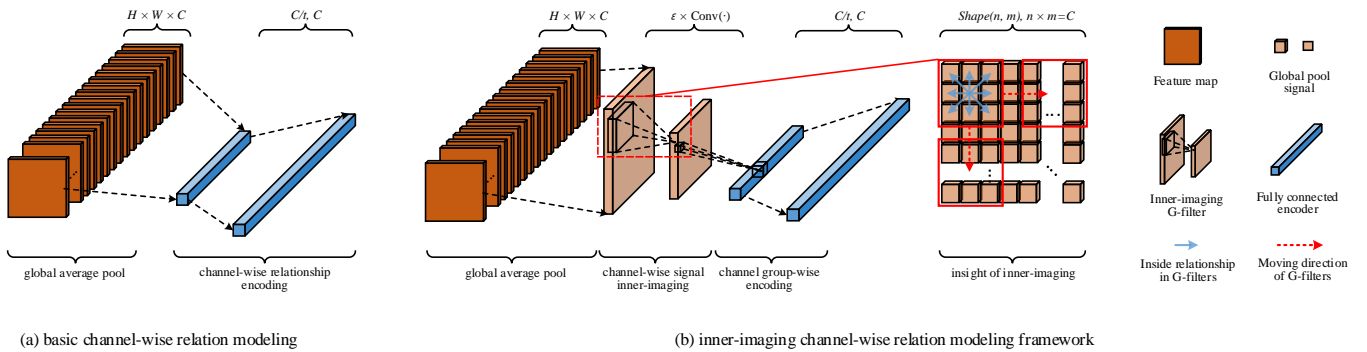


Fig. 1: Architectural comparison of channel relationship modeling. (a): The channel relation encoder with considering of identity mapping; (b): The Inner-Imaging channel-wise relationship modeling architecture, which organizes and models the channel relationships inside each group and between groups.

- The diversity of G-filters with different utility is explored. Moreover, it is also proposed that multi-shape G-filters can be integrated to realize the fusion of multi-size channel groups modeling.
- The InI mechanism is employed to some popular CNN structures. For residual networks (ResNets), it builds inner-imaged maps with both residual and identity mappings, enabling identity flows to participate in the attentional process of residual flows.
- With the InI mechanism, the effect of diverse channel grouping types is analyzed with the ablation studies for each mode of InI-model. Besides, the ability of the InI module to collaborate with the spatial attention mechanism [29], [30] is verified.

The remainder of this paper is organized as follows. Section II discusses related works. Section III introduces the overall framework of the InI mechanism and its enhanced edition for residual networks. Section IV presents our theoretical explanations for designing of the InI mechanism. Section V describes the experimental results and analysis. We conclude in Section VI.

II. RELATED WORKS

A. Efficient convolution structures

Both huge volume and calculation of CNNs [31], [32], [33], [34] are considered due to its serve redundancy [35], [36], which easily leads to inefficient modeling and overfitting. Some methods impose regularization constraints to the network features [37], [38], or random occlusion or perturbation of intermediate features [39], [40], some methods attempt to prune the block or channel for an over-complete convolutional architecture [41], [42], [43], or use an early exit mechanism [44]. They apply destructive simplification to some complete models, rather than increase the modeling efficiency of finite-scale models. These methods need to build an initial large-scale network and consume computation to optimize pruning operations.

In a parallel line, efficient use of existing components and features is a two-pronged approach [45], [46]. Some methods densely model the feature maps [47], [24], [48]. To make CNN channels organized well, the modeling of channel relationships

has attracted research attention [49]. Some approaches attempt to enhance the association of channels [50] and achieve high-efficiency performance by modeling them in grouping [20], [24]. The aforementioned studies only refine the features of the middle layers repetitively or train the convolution channels in fixed groups, and they do not use the channel relationships to re-scale the feature maps. Compared with them, the InI mechanism can model the channel grouping relationships with various sizes and use attention module to re-weight them.

B. Attention and gating mechanisms in CNNs

Attention is widely applied in the modeling process of CNNs [51]. It is typically used to model the spatial attentional area [52], [53], [54], [55] and content meaning [56], including multi-scale [57], [58] and multi-shape [59], [60] features. As a tool for biasing the allocation of resources [21], attention is also used to regulate the internal CNN features [61], [62]. Unlike channel switching, combination [63], [64], channel-wise attention provides an end-to-end training solution for re-weighting the intermediate channel features. It can be also combined with spatial attention in various ways, such as juxtaposition [29], sequential [30] or integrated [65].

The aforementioned studies either aggregate the features to complement each other or enhance the diversity of the feature maps after a simple encoder. In contrast, the Inner-Imaging design considers both synchronously. It firstly uses convolutional filters to organize channel signals on a pseudo-image, like we put lenses in the convolutional networks. This novel strategy reflects the grouping cooperative relations in multi-scale and achieves the integrated optimization of the diversity, complementarity, and completeness of CNN channels.

III. PROPOSED METHOD

In this section, the overall framework of the Inner-Imaging module is proposed, with single type of G-filter or combined multi-shape G-filters. Subsequently, the special version of InI module for ResNets is designed to jointly model the channel signals of residual flow and identity flow.

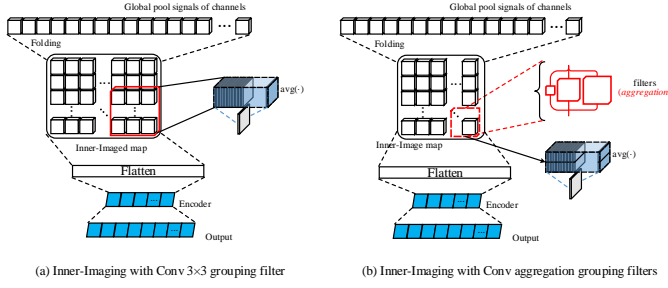


Fig. 2: The detailed structure of the Inner-Imaging. (a): The Inner-Imaging module with 3×3 convolutional G-filter; (b): The Inner-Imaging module with multi-shape G-filters aggregation.

A. Overall framework

In each layer of CNNs, each convolutional kernel produces a feature maps $\mathbf{u}_l^c \in \mathbb{R}^{W \times H}$, which is defined as a channel. It forms the basic unit of intermediate features in convolutional networks. To model the relationships between them, the feature maps \mathbf{u}_l^c is squeezed firstly, as follows:

$$\mathbf{u}_l^c \in \mathbf{U}_l = F_l(\mathbf{U}_{l-1}, \mathbf{W}_l) = [\mathbf{u}_l^1, \mathbf{u}_l^2, \dots, \mathbf{u}_l^C], \quad (1)$$

$$\hat{u}_l^c = F_{sq}(\mathbf{u}_l^c) = \frac{1}{W \times H} \sum_{i=1}^W \sum_{j=1}^H u_l^c(i, j), \quad (2)$$

$$\hat{\mathbf{v}}_{init} = [\hat{u}_l^1, \hat{u}_l^2, \dots, \hat{u}_l^C] \in \mathbb{R}^{1 \times C}, \quad (3)$$

where $\mathbf{U}_l = [\mathbf{u}_l^1, \mathbf{u}_l^2, \dots, \mathbf{u}_l^C]$ refers to the feature maps in the layer l and C is the number of channels, $F_l(\cdot)$ is the function of convolutional layer parameterized by \mathbf{W}_l , and $F_{sq}(\cdot)$ denotes the squeeze function with global average pooling. The channel signals $[\hat{u}_l^1, \hat{u}_l^2, \dots, \hat{u}_l^C]$ can be obtained from feature maps \mathbf{U}_l and the initial channel signal map $\hat{\mathbf{v}}_{init}$ with the shape of $(1 \times C)$ is also constructed.

Next, by scanning the channel signal map with G-filters $\mathbf{w}^{(a \times b)}$, the channels in the same receptive field with the shape of $(a \times b)$ are organized as a group. However, most G-filters are not available on the initial map $\hat{\mathbf{v}}_{init}$ unless $a = 1$. Therefore, a new map, named as the inner-imaged map, is generated as:

$$\begin{aligned} \hat{\mathbf{v}}_f &= T(\hat{\mathbf{v}}_{init}) = T([\hat{u}_l^1, \hat{u}_l^2, \dots, \hat{u}_l^C]) \\ &= \begin{bmatrix} \hat{u}_l^{11} & \dots & \hat{u}_l^{1M} \\ \vdots & \ddots & \vdots \\ \hat{u}_l^{N1} & \dots & \hat{u}_l^{NM} \end{bmatrix} \in \mathbb{R}^{N \times M}, (N \times M = C), \end{aligned} \quad (4)$$

where $\hat{\mathbf{v}}_f$ denotes the inner-imaged map which is folded by the reshape function $T(\cdot)$, its shape is $(N \times M)$. Then, the grouping relations between CNN channels are modeled as follows:

$$\mathbf{v}'[i] = \hat{\mathbf{v}}_f * \mathbf{w}_i^{(a \times b)} = \begin{bmatrix} v_i^{11} & \dots & v_i^{1m} \\ \vdots & \ddots & \vdots \\ v_i^{n1} & \dots & v_i^{nm} \end{bmatrix}, \quad (5)$$

$$\bar{v}^{xy} = \left(\sum_{i=1}^{\varepsilon} (v_i^{xy}) \right) / \varepsilon \quad (6)$$

$$\bar{\mathbf{v}}' = \frac{1}{\varepsilon} \sum_{i=1}^{\varepsilon} (\mathbf{v}'[i]) = \begin{bmatrix} \bar{v}^{11} & \dots & \bar{v}^{1m} \\ \vdots & \ddots & \vdots \\ \bar{v}^{n1} & \dots & \bar{v}^{nm} \end{bmatrix} \in \mathbb{R}^{n \times m} \quad (7)$$

$$\begin{aligned} \bar{\mathbf{v}} &= (F_{flatten}(\bar{\mathbf{v}}'))^T = [\bar{v}^1, \dots, \bar{v}^{C^g}]^T \in \mathbb{R}^{C^g \times 1} \\ &= [\bar{v}^{11}, \dots, \bar{v}^{1m}, \bar{v}^{21}, \dots, \bar{v}^{2m}, \dots, \bar{v}^{nm}]^T, \\ &(n \times m = C^g) \end{aligned} \quad (8)$$

In Eq. 5–8, the operator $*$ denotes the convolution and $\mathbf{v}'[i]$ refers to the convolutional result of G-filter $\mathbf{w}_i^{(a \times b)}$ on inner-imaged map, and its shape is $(n \times m)$, ε is the number of G-filters. The convolutional results are averaged and then applied to obtain the grouping map $\bar{\mathbf{v}}'$ whose element is \bar{v}^{xy} . Finally, the grouping map $\bar{\mathbf{v}}'$ is flatten as the tensor $\bar{\mathbf{v}} \in \mathbb{R}^{C^g \times 1}$, where each element of $\bar{\mathbf{v}}$ is a group signal modeled by $\mathbf{w}_i^{(a \times b)}$, and C^g is the number of modeled channel groups.

Obviously, the diversified multi-shape G-filters can be integrated such as $\{\mathbf{w}^{(a_1 \times b_1)}, \mathbf{w}^{(a_2 \times b_2)}, \dots, \mathbf{w}^{(a_p \times b_p)}\}$, which can be applied to organize the channel groups with different sizes as follows:

$$\mathbf{v}'_j[i] = (\hat{\mathbf{v}}_f * \mathbf{w}_i^{(a_j \times b_j)}) \in \mathbb{R}^{n_j \times m_j}, \quad (9)$$

$$\mathbf{v}'_{1:p}[i] = [\mathbf{v}'_1[i] \bowtie \mathbf{v}'_2[i] \bowtie \dots \bowtie \mathbf{v}'_p[i]], \quad (10)$$

$$\begin{aligned} \bar{\mathbf{v}}'_{1:p} &= \left(\frac{1}{\varepsilon} \sum_{i=1}^{\varepsilon} (\mathbf{v}'_{1:p}[i]) \right) \in \mathbb{R}^{(n_{1:p}) \times (m_{1:p})} \\ &, \quad n_{1:p} = \max_{j=1}^p (n_j), m_{1:p} = \sum_{j=1}^p (m_j), \end{aligned} \quad (11)$$

where $\mathbf{v}'_j[i]$ with the shape of $(n_j \times m_j)$ indicates the convolutional result of the G-filter $\mathbf{w}_i^{(a_j \times b_j)}$ and p is the number of types of G-filter. $\mathbf{v}'_{1:p}[i]$ is the concatenated result of all types G-filters and \bowtie means matrix concatenation. In the case of different shapes of matrix, zero is automatically filled into the blank. Then, $\bar{\mathbf{v}}'_{1:p}$ is the average result of each ε G-filters with different shapes and sizes. $((n_{1:p}) \times (m_{1:p}))$ is the final shape of averaged group signal map.

The grouping map is still flatten as:

$$\begin{aligned} \bar{\mathbf{v}} &= (F_{flatten}(\bar{\mathbf{v}}'_{1:p}))^T = [\bar{v}^1, \dots, \bar{v}^{C^g}]^T \in \mathbb{R}^{C^g \times 1}, \\ &((n_{1:p}) \times (m_{1:p}) = C^g) \end{aligned} \quad (12)$$

thus, a greater C^g than that in Eq. 8 is obtained, leading to more samples for the group relationships of CNN channels.

After representing the channel groups as $\bar{\mathbf{v}} \in \mathbb{R}^{C^g \times 1}$, the relations are encoded between group signals with FC layers $\mathbf{w}^1 \in \mathbb{R}^{\frac{C}{\varepsilon} \times C^g}$ and $\mathbf{w}^2 \in \mathbb{R}^{C \times \frac{C}{\varepsilon}}$. Then, the channel-wise attention is conducted as follows:

$$\mathbf{W}_{att} = \bigcup_{j=1}^p \{\mathbf{w}_1^{(a_j \times b_j)}, \dots, \mathbf{w}_\varepsilon^{(a_j \times b_j)}\} \cup \{\mathbf{w}^1, \mathbf{w}^2\}, \quad (13)$$

$$\mathbf{s} = F_{att}(\mathbf{U}_l, \mathbf{W}_{att}) = \sigma(\mathbf{w}^2 \cdot ReLU(\mathbf{w}^1 \cdot \bar{\mathbf{v}})) \quad (14)$$

$$\mathbf{U}_l^{att} = \mathbf{s} \circ \mathbf{U}_l = F_{att}(\mathbf{U}_l, \mathbf{W}_{att}) \circ F_l(\mathbf{U}_{l-1}, \mathbf{W}_l), \quad (15)$$

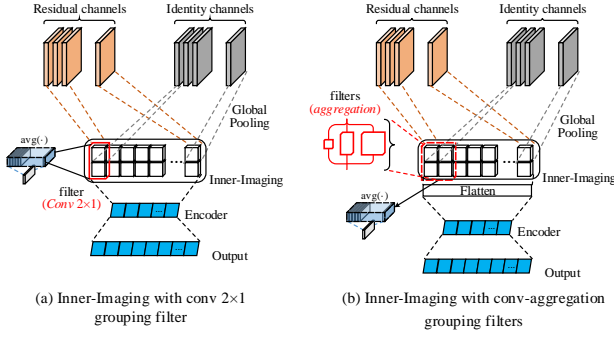


Fig. 3: The special version of simplified Inner-Imaging for ResNets. (a): The simplified Inner-Imaging module with 2×1 convolutional G-filter; (b): The simplified Inner-Imaging module with multi-shape G-filters aggregation.

where \mathbf{W}_{att} is the set of parameters in the InI module, which contains all parameters of the G-filters and the FC encoders, \mathbf{s} is the channel-wise attentional outputs, F_{att} denotes the summarized function of channel-wise attention, operator \circ is the elements-wise product and \mathbf{U}_l^{att} refers to the attentional feature maps. The number of G-filters ε is set to C/t , where t is the dimensionality-reduction ratio which is set to 16 as [21].

Fig. 2 shows the detailed structure of the InI module.

B. Special version for ResNets

In ResNets, the residual flow is considered as a complement to the identity mapping [66], inspired by this argument, we propose the special version of InI mechanism for ResNets, it attempt to expand the scope of channel relational modeling to both residual and identity channels, this strategy help residual mappings to supplement identity mappings more precisely.

We define the identity and residual mappings as \mathbf{X}_l and \mathbf{U}_l , respectively. The feature map \mathbf{x}_l^c in the identity mappings can be pooled in a similar way to Eq. 1. As shown in Fig. 3, the channel signals of \mathbf{X}_l and \mathbf{U}_l can be simply stacked without operation of folding, as follows:

$$\mathbf{x}_l^c \in \mathbf{X}_l = [\mathbf{x}_l^1, \mathbf{x}_l^2, \dots, \mathbf{x}_l^C], \quad (16)$$

$$\hat{x}_l^c = F_{sq}(\mathbf{x}_l^c) = \frac{1}{W \times H} \sum_{i=1}^W \sum_{j=1}^H x_l^c(i, j), \quad (17)$$

$$\hat{\mathbf{x}}_l = [\hat{x}_l^1, \hat{x}_l^2, \dots, \hat{x}_l^C] \in \mathbb{R}^{1 \times C}, \quad (18)$$

$$\hat{\mathbf{v}}_{stack} = \begin{bmatrix} \hat{\mathbf{U}}_l \\ \hat{\mathbf{x}}_l \end{bmatrix} = \begin{bmatrix} \hat{u}_l^1 & \hat{u}_l^2 & \dots & \hat{u}_l^C \\ \hat{x}_l^1 & \hat{x}_l^2 & \dots & \hat{x}_l^C \end{bmatrix} \in \mathbb{R}^{2 \times C}, \quad (19)$$

$$\bar{\mathbf{v}}' = \frac{1}{\varepsilon} \sum_{i=1}^{\varepsilon} \left(\hat{\mathbf{v}}_{stack} * \mathbf{w}_i^{(a \times b)} \right), \quad (a \leq 2), \quad (20)$$

$$\bar{\mathbf{v}} = \begin{cases} (\bar{\mathbf{v}}')^\top, & \text{if } a = 2 \\ (F_{flatten}(\bar{\mathbf{v}}'))^\top, & \text{if } a < 2 \end{cases} \in \mathbb{R}^{C^g \times 1} \quad (21)$$

where \hat{x}_l^c is the squeezed signal of identity feature maps x_l^c , $\hat{\mathbf{v}}_{stack}$ is the simplified inner-imaged map by stacking the

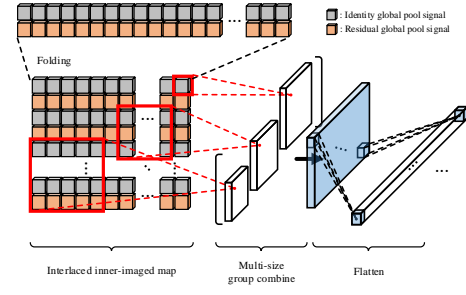


Fig. 4: The folded inner-imaged map of ResNets and the subsequent modeling with multi-shape G-filters.

channel signals $\hat{\mathbf{u}}_l$ and $\hat{\mathbf{x}}_l$. Multi-shape G-filters can also be applied to $\hat{\mathbf{v}}_{stack}$, as follows:

$$\bar{\mathbf{v}}' = \frac{1}{\varepsilon} \sum_{i=1}^{\varepsilon} \left(F_{norm} \left(\hat{\mathbf{v}}_{stack} * \mathbf{w}_i^{(a_1 \times b_1)}, \dots, \hat{\mathbf{v}}_{stack} * \mathbf{w}_i^{(a_p \times b_p)} \right) \right), \quad (\forall a_j : a_j \leq 2), \quad (22)$$

$$\bar{\mathbf{v}} = \begin{cases} (\bar{\mathbf{v}}')^\top, & \text{if } \forall a_j : a_j = 2 \\ (F_{flatten}(\bar{\mathbf{v}}'))^\top, & \text{if } \exists a_j : a_j < 2 \end{cases} \quad (23)$$

Although the step of folding the original channel signal map is omitted here, it has considerable limitation on the shape of group filters: $\forall a : a \leq 2$. So, we fold $\hat{\mathbf{v}}_{stack}$ as:

$$\begin{aligned} \hat{\mathbf{v}}_f &= T_{alt}(\hat{\mathbf{v}}_{stack}) = \begin{bmatrix} \hat{v}_f^{11} & \dots & \hat{v}_f^{1M} \\ \vdots & \ddots & \vdots \\ \hat{v}_f^{N1} & \dots & \hat{v}_f^{NM} \end{bmatrix} \\ &= T_{alt} \left(\begin{bmatrix} \hat{\mathbf{x}}_l \\ \hat{\mathbf{u}}_l \end{bmatrix} \right) = \begin{bmatrix} \hat{x}_l^1 & \hat{x}_l^2 & \dots & \hat{x}_l^m \\ \hat{u}_l^1 & \hat{u}_l^2 & \dots & \hat{u}_l^m \\ \vdots & \vdots & \ddots & \vdots \\ \hat{x}_l^{\frac{N}{2}1} & \hat{x}_l^{\frac{N}{2}2} & \dots & \hat{x}_l^{\frac{N}{2}M} \\ \hat{u}_l^{\frac{N}{2}1} & \hat{u}_l^{\frac{N}{2}2} & \dots & \hat{u}_l^{\frac{N}{2}M} \end{bmatrix} \\ &\in \mathbb{R}^{N \times M}, \quad (N \times M = 2C), \end{aligned} \quad (24)$$

where $\hat{\mathbf{v}}_f$ is the folded inner-imaged map with $\hat{\mathbf{x}}_l$ and $\hat{\mathbf{u}}_l$, T_{alt} is the alternating reshape function, which enables both residual and identity signals to be scanned in one receptive field.

Fig. 4 shows the structure of the special version InI module on folded inner-imaged map, with multi-shape G-filters aggregation. The subsequent process follows Eq. 9–11, the only difference is that the grouping relations of both residual and identity channels are modeled.

FC encoders $\mathbf{w}^1 \in \mathbb{R}^{\frac{C}{t} \times C^g}$ and $\mathbf{w}^2 \in \mathbb{R}^{C \times \frac{C}{t}}$ are still used to model the group-wise relations and output the final channel-wise attentional values. As the definition of residual unit [10]:

$$y = \mathbf{X}_l + \mathbf{U}_l = \mathbf{X}_l + F_{res}(\mathbf{X}_l, \mathbf{W}_l), \quad (25)$$

we obtain:

$$\mathbf{s} = F_{att}((\mathbf{X}_l, \mathbf{U}_l), \mathbf{W}_{att}), \quad (26)$$

$$\begin{aligned} y &= \mathbf{X}_l + \mathbf{s} \circ \mathbf{U}_l \\ &= \mathbf{X}_l + F_{att}((\mathbf{X}_l, \mathbf{U}_l), \mathbf{W}_{att}) \circ F_{res}(\mathbf{X}_l, \mathbf{W}_l), \end{aligned} \quad (27)$$

where \mathbf{s} refers to the outputs of channel-wise attention, and \mathbf{W}_{att} is the total set of parameters in InI module, which is defined by Eq. 13.

IV. THEORIES

In this section, some theoretical details of the InI model are elaborated and discussed, including its technical advantages and some insightful design motivations.

A. The insight of Inner-Imaging mechanism

It is an elegant design method to give new functions and meanings to existing tools. The convolutional filter is usually used to model the spatial features on vision data. Also, it can help us to model the grouping relations of convolutional channels very conveniently.

Compare with the typical channel-wise attention mechanism, the InI module can provide more complete and diverse modeling of channel relations, especially on grouping relations.

Excluding the output layer \mathbf{w}^2 , we discuss the FC encoder \mathbf{w}^1 , as follows:

$$\mathbf{w}^1 = \begin{bmatrix} w_1^{11} & \cdots & w_1^{1C} \\ \vdots & \ddots & \vdots \\ w_1^{\frac{C}{t}1} & \cdots & w_1^{\frac{C}{t}C} \end{bmatrix} \in \mathbb{R}^{\frac{C}{t} \times C}, \quad (28)$$

$$\begin{aligned} \mathbf{e} &= \mathbf{w}^1 \cdot (\hat{\mathbf{v}}_{init})^\top = \begin{bmatrix} w_1^{11} & \cdots & w_1^{1C} \\ \vdots & \ddots & \vdots \\ w_1^{\frac{C}{t}1} & \cdots & w_1^{\frac{C}{t}C} \end{bmatrix} \cdot \begin{bmatrix} \hat{u}_l^1 \\ \vdots \\ \hat{u}_l^C \end{bmatrix} \\ &= \left[\sum_{i=1}^C w_1^{1i} \hat{u}_l^i, \dots, \sum_{i=1}^C w_1^{\frac{C}{t}i} \hat{u}_l^i \right] \\ &= \left[e(\hat{\mathbf{v}}_{init}, \mathbf{w}_1^{1[\cdot]}) , \dots, e(\hat{\mathbf{v}}_{init}, \mathbf{w}_1^{\frac{C}{t}[\cdot]}) \right] \in \mathbb{R}^{1 \times \frac{C}{t}}, \end{aligned} \quad (29)$$

where \mathbf{e} denotes the embedding of CNN channels, $e(\cdot, \mathbf{w}_1^{i[\cdot]})$ indicates the feature parameterized by weights $\mathbf{w}_1^{i[\cdot]}$.

In InI mechanism, there are two successive stages: (a) grouping modeling; (b) FC embedding, as follows:

$$\begin{aligned} \mathbf{s} &= F_{att} \left(\mathbf{U}_l, \underbrace{\{\mathbf{w}^{(a_1 \times b_1)}, \dots, \mathbf{w}^{(a_p \times b_p)}\}}_a, \underbrace{\{\mathbf{w}^1, \mathbf{w}^2\}}_b \right), \\ & \left(\mathbf{w}^{(a_j \times b_j)} = [\mathbf{w}_1^{(a_j \times b_j)}, \dots, \mathbf{w}_\varepsilon^{(a_j \times b_j)}] \right), \end{aligned} \quad (30)$$

When the convolutions $\mathbf{w}_1^{(a_j \times b_j)}, \dots, \mathbf{w}_\varepsilon^{(a_j \times b_j)}$ are abbreviated as:

$$\sum_{i=1}^{\varepsilon} \left(\hat{\mathbf{v}}_f * \mathbf{w}_i^{(a_j \times b_j)} \right) \Rightarrow \hat{\mathbf{v}}_f * \mathbf{w}^{(a_j \times b_j)}, \quad (31)$$

we obtain:

$$\bar{\mathbf{v}}' = \hat{\mathbf{v}}_f * \mathbf{w}^{(a_1 \times b_1)} \bowtie \dots \bowtie \hat{\mathbf{v}}_f * \mathbf{w}^{(a_p \times b_p)} \quad (32)$$

$$\begin{aligned} \hat{\mathbf{v}}_f * \mathbf{w}^{(a_j \times b_j)} &= \begin{bmatrix} v^{11} & \cdots & v^{1m_j} \\ \vdots & \ddots & \vdots \\ v^{n_j 1} & \cdots & v^{n_j m_j} \end{bmatrix} \in \mathbb{R}^{n_j \times m_j} \\ &= \begin{bmatrix} e_g^j(\hat{\mathbf{g}}_j^1) & \cdots & e_g^j(\hat{\mathbf{g}}_j^{m_j}) \\ \vdots & \ddots & \vdots \\ e_g^j(\hat{\mathbf{g}}_j^{C_j^g - m_j + 1}) & \cdots & e_g^j(\hat{\mathbf{g}}_j^{C_j^g}) \end{bmatrix} \end{aligned} \quad (33)$$

$$\begin{aligned} \mathbf{w}^{(a_j \times b_j)} &= \left[[w_j^{11}, \dots, w_j^{1b_j}], \dots, [w_j^{a_j 1}, \dots, w_j^{a_j b_j}] \right] \\ &\Rightarrow [w_j^1, \dots, w_j^{\theta_j}], \quad (a_j \times b_j = \theta_j), \end{aligned} \quad (34)$$

$$\begin{aligned} \hat{\mathbf{g}}_j^k &= \left[[\hat{v}_{\rightarrow k}^{11}, \dots, \hat{v}_{\rightarrow k}^{1b_j}], \dots, [\hat{v}_{\rightarrow k}^{a_j 1}, \dots, \hat{v}_{\rightarrow k}^{a_j b_j}] \right] \\ &\Rightarrow [\hat{v}_k^1, \hat{v}_k^2, \dots, \hat{v}_k^{\theta_j}] \end{aligned} \quad (35)$$

$$\begin{aligned} e_g^j(\hat{\mathbf{g}}_j^k) &\Leftarrow e_g(\hat{\mathbf{g}}_j^k, \mathbf{w}^{(a_j \times b_j)}) \\ &= \sum_{x_k=1}^{a_j} \sum_{y_k=1}^{b_j} w_j^{x_k y_k} \hat{v}_f^{x_k y_k} = \sum_{i=1}^{\theta_j} w_j^i \hat{v}_k^i \end{aligned} \quad (36)$$

where θ_j is the number of parameters in the G-filter $\mathbf{w}^{(a_j \times b_j)}$. $\hat{\mathbf{g}}_j^k$ is the k -th receptive field of G-filter $\mathbf{w}^{(a_j \times b_j)}$, $\rightarrow k$ means that the G-filter slides to the k -th receptive field. $e_g^j(\cdot)$ is the encoded feature of each channel group.

Retrospect Eq. 29, it is noticed that the FC encoder is a particular form in Eq. 36, it has only one group which contains all channels.

Next, the role of FC layer \mathbf{w}^1 changes, as follows:

$$\begin{aligned} \mathbf{e} &= \mathbf{w}^1 \cdot \bar{\mathbf{v}} = \mathbf{w}^1 \cdot (F_{flatten}(\bar{\mathbf{v}}'))^\top \\ &= \left[\sum_{k=1}^{C_g} w_1^{1k} e_g(\hat{\mathbf{g}}^k), \dots, \sum_{k=1}^{C_g} w_1^{\frac{C}{t}k} e_g(\hat{\mathbf{g}}^k) \right], \end{aligned} \quad (37)$$

$$\Gamma(\hat{\mathbf{g}}_j^k) \in \{(a_j, b_j) : j = 1, 2, \dots, p\}, \quad (38)$$

$$\begin{aligned} \bar{\mathbf{v}} &= \left[e_g(\hat{\mathbf{g}}^1), \dots, e_g(\hat{\mathbf{g}}^{C_g}) \right] \\ &= \left[e_g^1(\hat{\mathbf{g}}_1^1), \dots, e_g^1(\hat{\mathbf{g}}_1^{C_g^1}) \right] \bowtie \dots \\ &\bowtie \left[e_g^p(\hat{\mathbf{g}}_p^1), \dots, e_g^p(\hat{\mathbf{g}}_p^{C_p^p}) \right], \quad (C_g = \sum_{j=1}^p C_g^j), \end{aligned} \quad (39)$$

where $\Gamma(\cdot)$ denotes the shape of matrix, and the one-hot G-filter $\mathbf{o} = [\alpha] \in \mathbb{R}^{1 \times 1}$ plays an important role. We obtain:

$$\begin{aligned} \hat{\mathbf{v}}_f * \mathbf{o} &= \begin{bmatrix} e_g(\hat{\mathbf{g}}_o^1) & \cdots & e_g(\hat{\mathbf{g}}_o^M) \\ \vdots & \ddots & \vdots \\ e_g(\hat{\mathbf{g}}_o^{C-M+1}) & \cdots & e_g(\hat{\mathbf{g}}_o^C) \end{bmatrix} \\ &\in \mathbb{R}^{N \times M}, \quad (N \times M = C), \end{aligned} \quad (40)$$

$$\hat{\mathbf{g}}_o^k = [\hat{v}_{\rightarrow k}^{11}] = [\hat{v}_f^{xy}], \quad (x \times y = k), \quad (41)$$

$$e_g(\hat{\mathbf{g}}_o^k) = \alpha \cdot \hat{v}_f^{xy} \propto \hat{u}_l^k \in \hat{\mathbf{v}}_{init}, \quad (42)$$

where \propto means proportional relationship, and $e_g(\hat{\mathbf{g}}_o^k)$ indicates the case of which single channel constructs a group. So,

$$\sum_{k=1}^{C_g} w_1^{ik} e_g(\hat{\mathbf{g}}^k) = \underbrace{\sum_{k=1}^C w_1^{ik} e_g(\hat{\mathbf{g}}_o^k)}_{\text{channels}} + \underbrace{\sum_{k=1}^{C_{-o}} w_1^{ik} e_g(\hat{\mathbf{g}}_{-o}^k)}_{\text{groups}} \quad (43)$$

, $(C_g - C = C_{-o})$,

where $-o$ indicates that non-one-hot G-filter \mathbf{o} .

It can be seen that in the two stages of the InI mechanism, **stage-a**: the G-filters generate channel groups in diversified shapes and model channel relations within them, as Eq. 32–36; **stage-b**: the function of FC encoder \mathbf{w}_1 is applied to modeling the relations between various channel groups, as Eq. 37–39. The design of one-hot G-filter \mathbf{o} adds the consideration of modeling the relationship between individual channels and channel groups, as Eq. 40–43.

It is obviously concluded that the modeled channel relations by the InI mechanism include and much more abundant than that of the typical strategy.

B. Joint modeling of residual and identity mappings

Another trick is proposed for the InI mechanism in ResNets, which is the joint modeling of residual and identity mappings. It is believed that this trick makes the ResNets more efficient.

As described in [66], the loss ζ is back-propagated (BP) as:

$$\begin{aligned} \frac{\partial \zeta}{\partial \mathbf{X}_l} &= \frac{\partial \zeta}{\partial \mathbf{X}_L} \frac{\partial \mathbf{X}_L}{\partial \mathbf{X}_l} \\ &= \frac{\partial \zeta}{\partial \mathbf{X}_L} \left(1 + \frac{\partial}{\partial \mathbf{X}_l} \sum_{i=l}^{L-1} F_{res}(\mathbf{X}_i, \mathbf{W}_i) \right), \end{aligned} \quad (44)$$

where L indicates any deeper residual unit, l indicates any shallower unit, and after using channel-wise attention, we obtain:

$$\begin{aligned} \frac{\partial \zeta}{\partial \mathbf{X}_l} &= \frac{\partial \zeta}{\partial \mathbf{X}_L} \left(1 + \frac{\partial}{\partial \mathbf{X}_l} \sum_{i=l}^{L-1} F_{att}(\mathbf{U}_i) \right. \\ &\quad \left. \circ F_{res}(\mathbf{X}_i, \mathbf{W}_i) \right) \\ &= \frac{\partial \zeta}{\partial \mathbf{X}_L} \left(1 + \sum_{i=l}^{L-1} \left(F_{res}(\mathbf{X}_i, \mathbf{W}_i) \frac{\partial F_{att}(\mathbf{U}_i)}{\partial \mathbf{X}_l} \right. \right. \\ &\quad \left. \left. + F_{att}(\mathbf{U}_i) \frac{\partial F_{res}(\mathbf{X}_i, \mathbf{W}_i)}{\partial \mathbf{X}_l} \right) \right), \end{aligned} \quad (45)$$

because $\mathbf{U}_i = F_{res}(\mathbf{X}_i, \mathbf{W}_i)$, we obtain:

$$\begin{aligned} \frac{\partial \zeta}{\partial \mathbf{X}_l} &= \frac{\partial \zeta}{\partial \mathbf{X}_L} \left(1 + \sum_{i=l}^{L-1} \left(\mathbf{U}_i \frac{\partial F_{att}(\mathbf{U}_i)}{\partial \mathbf{X}_l} \right. \right. \\ &\quad \left. \left. + F_{att}(\mathbf{U}_i) \frac{\partial \mathbf{U}_i}{\partial \mathbf{X}_l} \right) \right) \\ &= \frac{\partial \zeta}{\partial \mathbf{X}_L} \left(1 + \sum_{i=l}^{L-1} \left(\mathbf{U}_i \frac{\partial F_{att}(\mathbf{U}_i)}{\partial \mathbf{U}_i} \frac{\partial \mathbf{U}_i}{\partial \mathbf{X}_l} \right. \right. \\ &\quad \left. \left. + F_{att}(\mathbf{U}_i) \frac{\partial \mathbf{U}_i}{\partial \mathbf{X}_l} \right) \right), \end{aligned} \quad (46)$$

where

$$\beta = \mathbf{U}_i \frac{\partial F_{att}(\mathbf{U}_i)}{\partial \mathbf{U}_i} + F_{att}(\mathbf{U}_i),$$

we obtain:

$$\frac{\partial \zeta}{\partial \mathbf{X}_l} = \frac{\partial \zeta}{\partial \mathbf{X}_L} \left(1 + \sum_{i=l}^{L-1} \left(\beta \cdot \frac{\partial \mathbf{U}_i}{\partial \mathbf{X}_l} \right) \right), \quad (47)$$

then, with our strategy, we obtain:

$$\begin{aligned} \frac{\partial \zeta}{\partial \mathbf{X}_l} &= \frac{\partial \zeta}{\partial \mathbf{X}_L} \left(1 + \frac{\partial}{\partial \mathbf{X}_l} \sum_{i=l}^{L-1} F_{att}(\mathbf{X}_i, \mathbf{U}_i) \right. \\ &\quad \left. \circ F_{res}(\mathbf{X}_i, \mathbf{W}_i) \right) \\ &= \frac{\partial \zeta}{\partial \mathbf{X}_L} \left(1 + \sum_{i=l}^{L-1} \left(F_{res}(\mathbf{X}_i, \mathbf{W}_i) \frac{\partial F_{att}(\mathbf{X}_i, \mathbf{U}_i)}{\partial \mathbf{X}_l} \right. \right. \\ &\quad \left. \left. + F_{att}(\mathbf{X}_i, \mathbf{U}_i) \frac{\partial F_{res}(\mathbf{X}_i, \mathbf{W}_i)}{\partial \mathbf{X}_l} \right) \right) \\ &= \frac{\partial \zeta}{\partial \mathbf{X}_L} \left(1 + \sum_{i=l}^{L-1} \left(\mathbf{U}_i \frac{\partial F_{att}(\mathbf{X}_i, \mathbf{U}_i)}{\partial \mathbf{X}_l} \right. \right. \\ &\quad \left. \left. + F_{att}(\mathbf{X}_i, \mathbf{U}_i) \frac{\partial \mathbf{U}_i}{\partial \mathbf{X}_l} \right) \right) \\ &= \frac{\partial \zeta}{\partial \mathbf{X}_L} \left(1 + \sum_{i=l}^{L-1} \left(\mathbf{U}_i \left(\frac{\partial F_{att}(\mathbf{X}_i, \mathbf{U}_i)}{\partial \mathbf{U}_i} \frac{\partial \mathbf{U}_i}{\partial \mathbf{X}_l} \right. \right. \right. \\ &\quad \left. \left. + \frac{\partial F_{att}(\mathbf{X}_i, \mathbf{U}_i)}{\partial \mathbf{X}_i} \frac{\partial \mathbf{X}_i}{\partial \mathbf{X}_l} \right) \right. \\ &\quad \left. \left. + F_{att}(\mathbf{X}_i, \mathbf{U}_i) \frac{\partial \mathbf{U}_i}{\partial \mathbf{X}_l} \right) \right), \end{aligned} \quad (48)$$

in which we set

$$\beta = \mathbf{U}_i \frac{\partial F_{att}(\mathbf{X}_i, \mathbf{U}_i)}{\partial \mathbf{U}_i} + F_{att}(\mathbf{U}_i),$$

and

$$\gamma = \mathbf{U}_i \frac{\partial F_{att}(\mathbf{X}_i, \mathbf{U}_i)}{\partial \mathbf{X}_i},$$

so, after sorting out Eq. 48, we obtain:

$$\frac{\partial \zeta}{\partial \mathbf{X}_l} = \frac{\partial \zeta}{\partial \mathbf{X}_L} \left(1 + \sum_{i=l}^{L-1} \left(\underbrace{\beta \cdot \frac{\partial \mathbf{U}_i}{\partial \mathbf{X}_l}}_{\propto \nabla \mathbf{U}_i} + \underbrace{\gamma \cdot \frac{\partial \mathbf{X}_i}{\partial \mathbf{X}_l}}_{\propto \nabla \mathbf{X}_i} \right) \right), \quad (49)$$

where the gradients of residual and identity mappings are denoted by $\nabla \mathbf{U}_i$ and $\nabla \mathbf{X}_i$. By using the strategy of joint modeling for residual and identity flows, the trade-off process of identity and residual mappings can be integrated into the BP optimization, so that residual flows can provide more efficient complementary modeling for identity mappings.

V. EXPERIMENTS

In this section, lots of experiments are conducted to verify the performance of the proposed methods. Firstly, the datasets and implementation details of networks are introduced. Secondly, the effects of different types of Inner-Imaging are analyzed, while the ablation study for various subassemblies of the InI module is conducted. Thirdly, comparisons of our models with state-of-the-art results are provided. Finally, we give the discussions of experimental results.

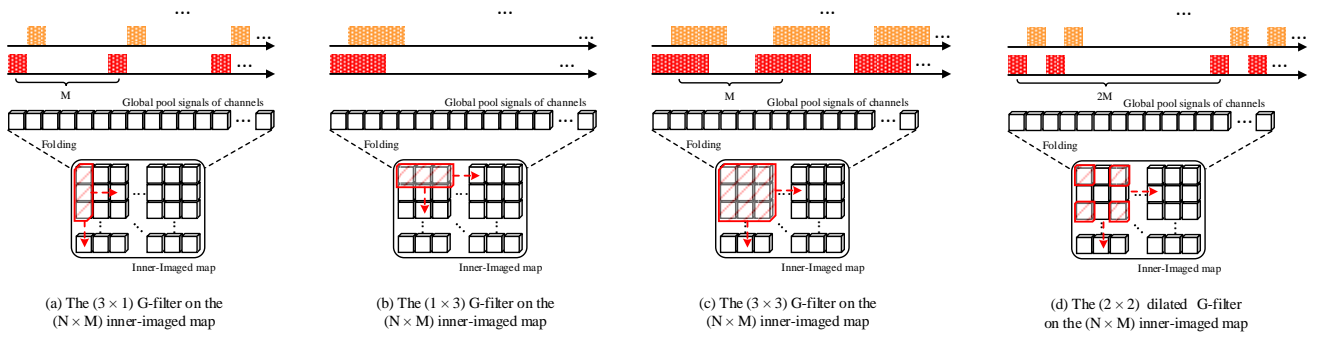


Fig. 5: Examples of channel grouping organization for multiple types of G-filters. (a): The G-filter with a vertical shape; (b): The G-filter with the horizontal shape with a horizontal shape; (c): The square G-filter; (d): The dilated G-filter.

TABLE I: Various types of G-filter sets.

Type	Name	Set of G-filters
Square	square-1	$\{(3 \times 3)\}$
	square-2	$\{(1 \times 1), (3 \times 3)\}$
	square-3	$\{(1 \times 1), (3 \times 3), (5 \times 5)\}$
	square-4	$\{(1 \times 1), (2 \times 2), (3 \times 3), (5 \times 5)\}$
	square-5	$\{(1 \times 1), (2 \times 2), (3 \times 3), (4 \times 4), (5 \times 5)\}$
Mix	mix-1	$\{(3 \times 3)\}$
	mix-2	$\{(1 \times 5), (3 \times 3)\}$
	mix-3	$\{(1 \times 5), (3 \times 3), (5 \times 1)\}$
	mix-4	$\{(1 \times 1), (1 \times 5), (3 \times 3), (5 \times 1)\}$
	mix-5	$\{(1 \times 1), (1 \times 5), (3 \times 3), (5 \times 1), (5 \times 5)\}$
Horizontal	horizon- n	$\{(1 \times 1), \dots, (1 \times n)\}$
Vertical	vertical- n	$\{(1 \times 1), \dots, (n \times 1)\}$
Simplified ^a	simple-1	$\{(2 \times 1)\}$
	simple-3	$\{(1 \times 1), (2 \times 1), (2 \times 2)\}$
Dilated ^b	d	$\{\dots, (5 \times 5, s = 2)\}$

^aUsed only for simplified version of InI module in ResNets.

^bUsed only in conjunction with other types of G-filters, not separately.

A. Datasets

As CIFAR-10, CIFAR-100, SVHN, and ImageNet are often used as benchmark datasets in image recognition experiments, they are also used here.

CIFAR-10 and CIFAR-100 [67]. The two datasets consist of 32×32 colored images. Both of them contain 60000 images divided equally into 10 and 100 classes, there are 50000 training images and 10000 for testing. The standard data augmentation (translation/mirroring) widely adopted as [10] is used for training sets.

SVHN [68]. The street view house numbers dataset contains 32×32 colored images of 73257 samples in the training set and 26032 for testing, with 531131 digits for additional training. Here all training data are used without data augmentation.

ImageNet [69]. It is used in ILSVRC 2012, which contains 1.2 million training images, 50000 validation images, and 100000 for testing, with 1000 classes. Standard data augmentation is adopted for the training set and the 224×224 crop is randomly sampled. All images are normalized into $[0, 1]$, with mean values and standard deviations.

B. Implementation Details

Networks. The proposed InI module is applied to several popular CNN networks that are taken as backbones, including: All Convolutional Net (All-CNN) [70], Pre-act Residual Net-

work (ResNet) [66], Wide Residual Network (WRN) [34], Pyramidal Residual Networks (PyramidNet) [71]. All the default settings of the backbones are followed. The proposed method is also compared with typical channel-wise attention [21] using the same backbones. The batch normalization [72] is performed following G-filters. Our implementation is based on MXNet and GluonCV¹

Training. The SGD with 0.9 Nesterov momentum is used to train models for 400 epochs on CIFAR and 80 epochs on SVHN, where the batch-size is 128. The learning rate starts at 0.1 and is divided by 10 at 50%, 75% and 90% of the number of total epochs. On ImageNet, we train models for 120 epochs with the batch size of 128, the initial learning rate is 0.1 and reduced by 10 at epochs 30, 60, and 90.

Settings of the InI Module. Since the size of the inner-imaged map needs to be taken into account in the setting of the G-filter, it follows rules as: if the receptive field of any G-filter exceeds the size of the inner-imaged map in any layer, the G-filter will be automatically discarded.

For the inner-imaged maps, their shapes are defined close to a square, for example: $(n = 2C/16, m = 16)$ for ResNet and $(n = 20, m = C/10)$ for WRN. The effects of size changes of the inner-imaged maps are tested on classification performance. For all kinds of ResNet, the special version of the InI module is used by default, which is introduced in Section III-B. It jointly models the identity and residual mappings.

In the following sections, the following naming rules are used rules for the proposed model: 1. the prefix "InI" is used to the name of the model using the internal imaging module; 2. for different G-filter types, the model name is attached with the type name as the suffix, where the type names of G-filters are listed in Table I.

C. Analysis of Different Inner-Imaging Types

Effects of the shape of G-filter. As the core component of the InI framework, these issues are needed to investigate: whether different G-filter combinations will have a serious impact on model performance (including the number and shape of G-filter), and what strategies can be applied to find the better combinations of G-filters.

As listed in Table I, a variety of G-filter combinations are designed, including square, slender (vertical and horizontal),

¹<https://gluon-cv.mxnet.io>

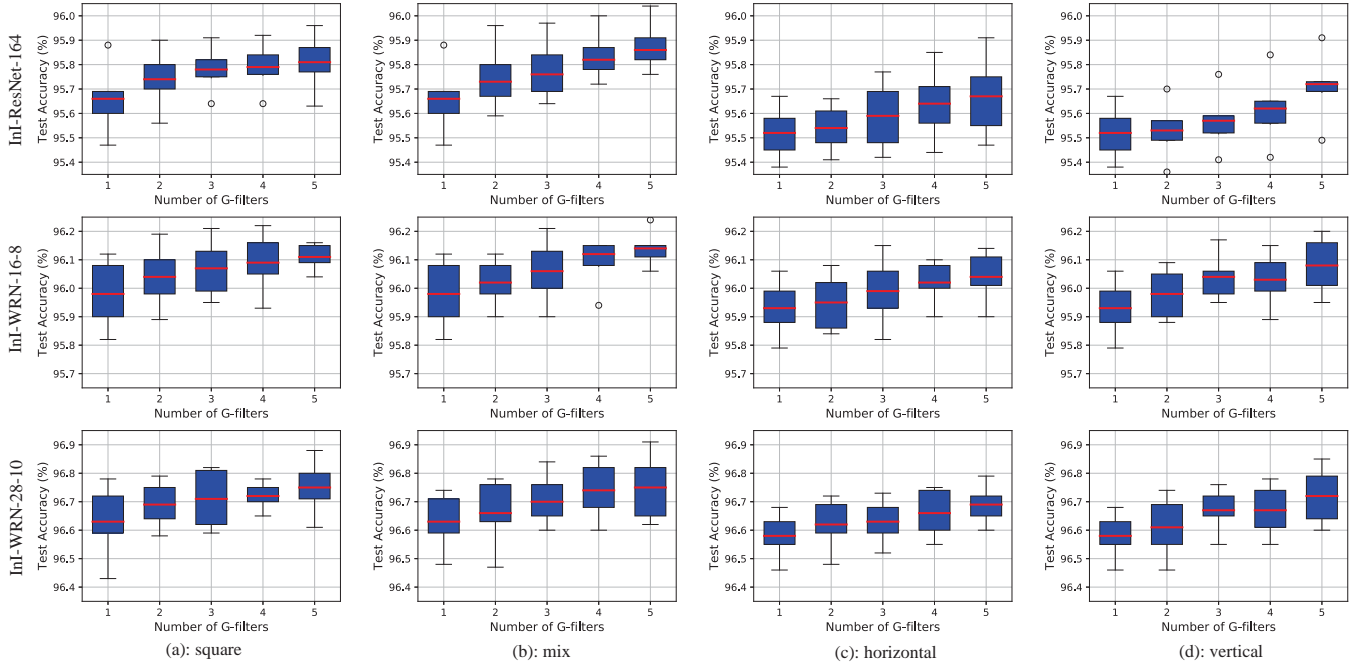


Fig. 6: Test accuracy curves by InI-ResNet and InI-WRN concerning G-filters with various types on CIFAR-10, the results are reported over 5 runs. For each column. (a): The square type; (b): The mix type; (c): The horizontal type; (d): The vertical type.

and mixed cases, these combinations are applied to the InI models so as to observe their performance changes in different settings, as shown in Fig. 6.

It can be seen from Fig. 6 that the performance of the InI module increases with the number of G-filters. Secondly, the performance of the types of square and mix G-filters is generally better than that of horizontal and vertical G-filters. Particularly, when the number of square G-filters is relatively large, the performance growth rate tends to be flat, and when the number of mixed G-filters is large, better results can be obtained. These indicate that the diversity of G-filter types can bring benefits to the InI model. Moreover, as deduced in Section IV-A, when we add the (1×1) G-filter to the G-filter set, a more obvious performance improvement can be obtained, which verifies the effect of the special group which only contains one channel, as Eq. 49.

Fig. 5 can help us analyze the above results, which illustrates the corresponding channel distribution of groups obtained by using G-filters with various shapes, on the original channel sequence. In the group of channels formed by horizontal and vertical G-filters, the former only contains adjacent channels, while the latter contains channels with slightly distant intervals. These monotonous grouping strategies lead to their mediocre performance. In the channel group formed by square G-filter, there are adjacent channels and distant channels. However, as the size of G-filter increases, the coverage of square G-filter becomes wider and wider, too many square G-filters also reduce the diversity of channel groups. In contrast, the mixed set G-filter composed of horizontal, vertical and square G-filters is more effective.

It can be also observed from Fig. 5(d) that the dilated [73] G-filter can use fewer parameters than square G-filter to complete a large scope of channel scanning, while overcoming the

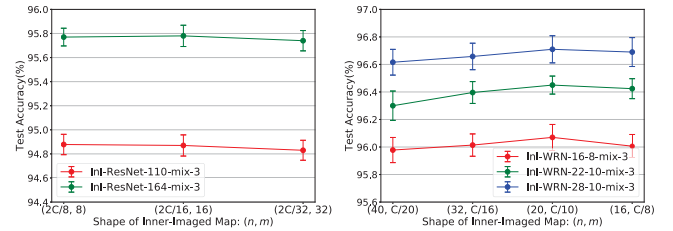


Fig. 7: Test accuracy curves by InI-ResNet (left) and InI-WRN on CIFAR-10, concerning the shape of inner-imaged map.

TABLE II: Comparison results of InI-models with or without dilated G-filter over 5 runs.

Model	Add dilated G-filter	CIFAR-10
InI-ResNet-164-square-3	no	4.22 ± 0.09
InI-ResNet-164-square-3-d	yes	4.17 ± 0.11
InI-ResNet-164-mix-5	no	4.14 ± 0.09
InI-ResNet-164-mix-5-d	yes	4.10 ± 0.12
InI-WRN-16-8-square-3	no	3.93 ± 0.05
InI-WRN-16-8-square-3-d	yes	3.87 ± 0.12
InI-WRN-16-8-mix-5	no	3.86 ± 0.06
InI-WRN-16-8-mix-5-d	yes	3.81 ± 0.07
InI-WRN-28-10-square-3	no	3.29 ± 0.07
InI-WRN-28-10-square-3-d	yes	3.25 ± 0.13
InI-WRN-28-10-mix-5	no	3.25 ± 0.08
InI-WRN-28-10-mix-5-d	yes	3.22 ± 0.06

redundancy caused by high overlap rate between channel groups. The comparison results of the InI models with or without dilated G-filter are presented in Table II. It can be seen that the dilated G-filter help the InI-models improve further on the original bases.

Overall, combining G-filters with multiple sizes and shapes can indeed bring better modeling capabilities to the InI

TABLE III: Test error ((mean \pm std) %) of All-CNN, ResNet, SE-ResNet and multiple modes of InI-models over 5 runs on CIFAR-10 and CIFAR-100. Results that surpass all competing methods are **bold** and the overall best results are **red**.

Model	Joint	Aggregation	Fold	Dilated	Params.	CIFAR-10	CIFAR-100
All-CNN [70]	–	–	–	–	1.30M	7.25	33.71
SE-All-CNN [21]	–	–	–	–	1.35M	6.55 \pm 0.17	32.83 \pm 0.24
InI-All-CNN-square-1 (ours)	–	–	✓	–	1.35M	6.15 \pm 0.12	32.15 \pm 0.12
InI-All-CNN-square-3 (ours)	–	✓	✓	–	1.36M	6.06 \pm 0.14	32.02 \pm 0.21
ResNet-110 [66]	–	–	–	–	1.70M	6.37	–
ResNet-164 [66]	–	–	–	–	1.70M	5.46	24.33
SE-ResNet-110 [21]	–	–	–	–	1.75M	5.62 \pm 0.18	25.69 \pm 0.28
SE-ResNet-164 [21]	–	–	–	–	1.95M	4.79 \pm 0.09	22.43 \pm 0.21
InI-ResNet-110-square-1* (ours)	–	–	✓	–	1.70M	5.43 \pm 0.11	25.22 \pm 0.14
InI-ResNet-110-simple-1 (ours)	✓	–	–	–	1.75M	5.33 \pm 0.07	25.10 \pm 0.10
InI-ResNet-110-simple-3 (ours)	✓	✓	–	–	1.77M	5.22 \pm 0.18	24.98 \pm 0.27
InI-ResNet-110-square-1 (ours)	✓	–	✓	–	1.76M	5.20 \pm 0.12	24.95 \pm 0.14
InI-ResNet-110-square-3 (ours)	✓	✓	✓	–	1.77M	5.13 \pm 0.12	24.88 \pm 0.11
InI-ResNet-110-square-3-d (ours)	✓	✓	✓	✓	1.77M	5.09 \pm 0.08	24.81 \pm 0.13
InI-ResNet-164-square-1* (ours)	–	–	✓	–	1.88M	4.57 \pm 0.09	22.09 \pm 0.17
InI-ResNet-164-simple-1 (ours)	✓	–	–	–	1.95M	4.48 \pm 0.13	21.76 \pm 0.16
InI-ResNet-164-simple-3 (ours)	✓	✓	–	–	2.02M	4.32 \pm 0.18	21.63 \pm 0.10
InI-ResNet-164-square-1 (ours)	✓	–	✓	–	1.99M	4.34 \pm 0.15	21.60 \pm 0.12
InI-ResNet-164-square-3 (ours)	✓	✓	✓	–	2.02M	4.22 \pm 0.09	21.52 \pm 0.20
InI-ResNet-164-square-3-d (ours)	✓	✓	✓	✓	2.02M	4.17 \pm 0.11	21.46 \pm 0.18
InI-ResNet-164-mix-5 (ours)	✓	✓	✓	–	2.04M	4.14 \pm 0.09	21.39 \pm 0.22
InI-ResNet-164-mix-5-d (ours)	✓	✓	✓	✓	2.04M	4.10 \pm 0.12	21.33 \pm 0.17

*Without joint modeling of residual and identity mappings in ResNets.

TABLE IV: Test error ((mean \pm std) %) of WRN, SE-WRN and multiple modes of InI-models over 5 runs on CIFAR-10 and CIFAR-100. Results that surpass all competing methods are **bold** and the overall best results are **red**.

Model	Joint	Aggregation	Fold	Dilated	Params.	CIFAR-10	CIFAR-100
WRN-22-10 [34]	–	–	–	–	26.80M	4.44	20.75
WRN-28-10 [34]	–	–	–	–	36.50M	4.17	20.50
SE-WRN-16-8 [21]	–	–	–	–	11.10M	4.59 \pm 0.11	20.97 \pm 0.16
SE-WRN-22-10 [21]	–	–	–	–	27.05M	4.05 \pm 0.15	19.50 \pm 0.08
SE-WRN-28-10 [21]	–	–	–	–	36.80M	3.79 \pm 0.09	19.01 \pm 0.18
InI-WRN-16-8-simple-3 (ours)	✓	✓	–	–	11.14M	4.02 \pm 0.16	19.28 \pm 0.18
InI-WRN-16-8-square-1 (ours)	✓	–	✓	–	11.10M	4.02 \pm 0.08	19.30 \pm 0.08
InI-WRN-16-8-square-3 (ours)	✓	✓	✓	–	11.14M	3.93 \pm 0.05	19.17 \pm 0.11
InI-WRN-16-8-square-3-d (ours)	✓	✓	✓	✓	11.14M	3.87 \pm 0.12	19.12 \pm 0.11
InI-WRN-16-8-mix-5 (ours)	✓	✓	✓	–	11.20M	3.86 \pm 0.06	19.10 \pm 0.07
InI-WRN-16-8-mix-5-d (ours)	✓	✓	✓	✓	11.20M	3.81 \pm 0.07	19.03 \pm 0.09
InI-WRN-22-10-simple-3 (ours)	✓	✓	–	–	27.12M	3.66 \pm 0.09	18.41 \pm 0.17
InI-WRN-22-10-square-1 (ours)	✓	–	✓	–	27.10M	3.64 \pm 0.14	18.44 \pm 0.13
InI-WRN-22-10-square-3 (ours)	✓	✓	✓	–	27.12M	3.55 \pm 0.03	18.37 \pm 0.15
InI-WRN-22-10-square-3-d (ours)	✓	✓	✓	✓	27.12M	3.49 \pm 0.06	18.31 \pm 0.09
InI-WRN-22-10-mix-5 (ours)	✓	✓	✓	–	27.16M	3.51 \pm 0.08	18.31 \pm 0.10
InI-WRN-22-10-mix-5-d (ours)	✓	✓	✓	✓	27.16M	3.48 \pm 0.07	18.26 \pm 0.11
InI-WRN-28-10-square-1* (ours)	–	–	✓	–	36.60M	3.49 \pm 0.12	18.49 \pm 0.11
InI-WRN-28-10-simple-1 (ours)	✓	–	–	–	36.80M	3.43 \pm 0.10	18.33 \pm 0.16
InI-WRN-28-10-simple-3 (ours)	✓	✓	–	–	36.85M	3.35 \pm 0.05	18.27 \pm 0.14
InI-WRN-28-10-square-1 (ours)	✓	–	✓	–	36.82M	3.37 \pm 0.10	18.28 \pm 0.13
InI-WRN-28-10-square-3 (ours)	✓	✓	✓	–	36.88M	3.29 \pm 0.07	18.11 \pm 0.17
InI-WRN-28-10-square-3-d (ours)	✓	✓	✓	✓	36.88M	3.25 \pm 0.13	18.05 \pm 0.13
InI-WRN-28-10-mix-5 (ours)	✓	✓	✓	–	36.90M	3.25 \pm 0.08	18.03 \pm 0.06
InI-WRN-28-10-mix-5-d (ours)	✓	✓	✓	✓	36.90M	3.22 \pm 0.06	17.96 \pm 0.15

*Without joint modeling of residual and identity mappings in ResNets.

mechanisms. The effect on the performance of different G-filter type selection is very small. Although the maximum performance of InI can be achieved by combining G-filters of various shapes as much as possible, we can get very competitive performance by just integrating three G-filters, like G-filter type "square-3-d".

Effects of the shape of inner-imaged map. We compare the different shapes of the folded inner-imaged maps, which causes little fluctuations in classification results, as shown in Fig. 7, the inner-imaged map closer to the square shows slightly better results.

In subsequent experiments, the shape of inner-imaged maps is taken as ($n = 20, m = C/10$) for WRN, ($n = 8, m = C/8$) for All-CNN and ($n = 2C/16, m = 16$) for other backbones.

D. Ablation Studies

It is reasonable to study the effects of all tricks used in the InI models, which include: (1) Jointly modeling from identity and residual mappings (Joint); (2) Multi-shape G-filter aggregation (Aggregation); (3) Folded inner-imaged map (Fold); (4) Add dilated G-filter. These tricks are gradually added to the same backbone.

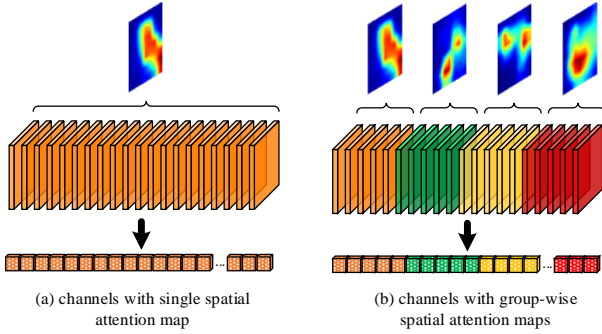


Fig. 8: The illustrations of spatial attention. (a): Single spatial attention; (b): Group-wise multiple spatial attention.

As listed in Tables III and IV, the best records with the same backbone are in bold and the best results are highlighted in red. As the components are gradually added, the test error continues to decrease, and the fully configured InI-models achieved the best results. Besides, many small-scale InI-models achieve performance close to or even better than the larger-scale typical models. Every trick in our InI mechanism including shows the improvements on classification results.

It can be found that the well-configured (with 3 or more proposed tricks) InI models can improve the typical channel-wise attention network by nearly 0.6%. Compared with SE-Net, the InI-models can bring about much more performance improvement.

E. Coordination with Spatial Attention

The spatial attention mechanism [30] is a strategy to dynamically adjust the pixel-level weights on the feature maps. In this section, the cooperative ability of the proposed InI mechanism for spatial attention models is validated.

We use the InI module after conducting the spatial attentional operation as follows, and the spatial attention map (SP map) is recorded as ξ ,

$$\mathbf{U}_l^{new} = \mathbf{s} \circ F_{spa}(\mathbf{U}_l, \xi) = [\xi \circ \mathbf{u}_l^1, \dots, \xi \circ \mathbf{u}_l^C] \quad (50)$$

where $F_{spa}(\cdot)$ is the function of spatial attention and \mathbf{U}_l^{new} is the final feature matrix in layer l .

As shown in Fig. 8, multiple SP maps $\{\xi^1, \dots, \xi^\tau\}$ are also introduced on several divided channel groups to highlight the function of InI model, as:

$$\begin{aligned} \mathbf{U}_l^{new} &= \mathbf{s} \circ F_{spa}(\mathbf{U}_l, \{\xi^1, \dots, \xi^\tau\}) \\ &= [\xi^1 \circ \mathbf{u}_l^1, \dots, \xi^1 \circ \mathbf{u}_l^{\frac{C}{\tau}}, \dots \\ &\quad, \xi^\tau \circ \mathbf{u}_l^{C - \frac{C}{\tau} + 1}, \dots, \xi^\tau \circ \mathbf{u}_l^C] \end{aligned} \quad (51)$$

Fig. 9 shows the growth of parameters and test accuracy on CIFAR-10 when using different numbers of SP maps. It is noted that the InI model fits well with the spatial attention mechanism and gets better results than other methods. As the number of SP maps increases, the increments of parameters rise exponentially, and the performance of the model also improves, but when the number of SP maps reaches 8, the performance growth becomes less noticeable or even slightly declined.

The possible reason is that too many SP maps lead to some over-fitting on CIFAR-10 composed with small pictures.

F. Comparison Results

Table V reports the comparison results between the InI-models and state-of-the-art networks. It can be noticed that the InI-model obviously improve the performance of the baseline method, and the InI-PyramidNet-mix-5-d outperforms state-of-the-art results and achieves the best results on CIFAR-100 and achieves the second-best performance on CIFAR-10. Although the results of the InI-PyramidNet-square-3 are slightly lower, they achieve the third-best and second-best results on CIFAR-10 and CIFAR-100. The InI-WRN-square-3, InI-WRN-mix-5 and InI-WRN-mix-5-d are also very competitive and two of them achieve the best and second-best performance on SVHN.

The proposed InI-models have a general and fairly significant performance improvement for the corresponding backbone networks, requiring only little additional parameters and computations. We can infer that InI-models have a better convolutional component organization, so that convolution kernels can reflect the diversity, complementarity and overall completeness, thus avoiding the redundancy of feature maps and enhancing the integrity of feature representation.

The experimental results on ImageNet are listed in Table VI and the best results are highlighted in bold. It can be seen that InI-ResNet-50-mix-5-d improve the top-1 and top-5 error rate than SE-ResNet-50 by 1.21% and 0.85% respectively. InI-ResNet-101-mix-5-d exceeds SE-ResNet-101 by 1.04% and 0.8% respectively, which is even better than the performance of SE-ResNet-152. Compared the networks with mechanisms of both channel-wise attention and spatial attention, the InI-ResNet-mix-5-d without spatial attention strategy can obtain better performance than CBAM-ResNet with spatial attention. The results of our InI-ResNet-mix-5-d + spa \times 4 improve that of CBAM-ResNet by 0.9% \sim 1.5% on top-1 and 0.6% \sim 0.9% on top-5. Similarly, the smaller InI-models still defeat the larger compared models.

Fig. 10 illustrates some thermal visualization results of feature maps on ImageNet with different models. It can be found that the InI model can focus more accurately and completely on recognition objects.

The above results on ImageNet show the InI model also works well in large-scale image recognition tasks.

G. Discussions

Our experimental results show that the InI model can improve the modeling ability of CNN, especially for smaller convolution structures. The InI mechanism can fully stimulate their potential and make the classification results close to or even exceed the original larger CNN models. Besides, the InI model only needs very few additional parameters.

The performance improvement of the InI model than traditional channel attention mechanism validates the necessity of channel group relationship modeling and the superior modeling ability of the InI model for diversified channel relationships.

In experiments, many possibilities for the implementation of the InI mechanism are discussed. However, it does not mean

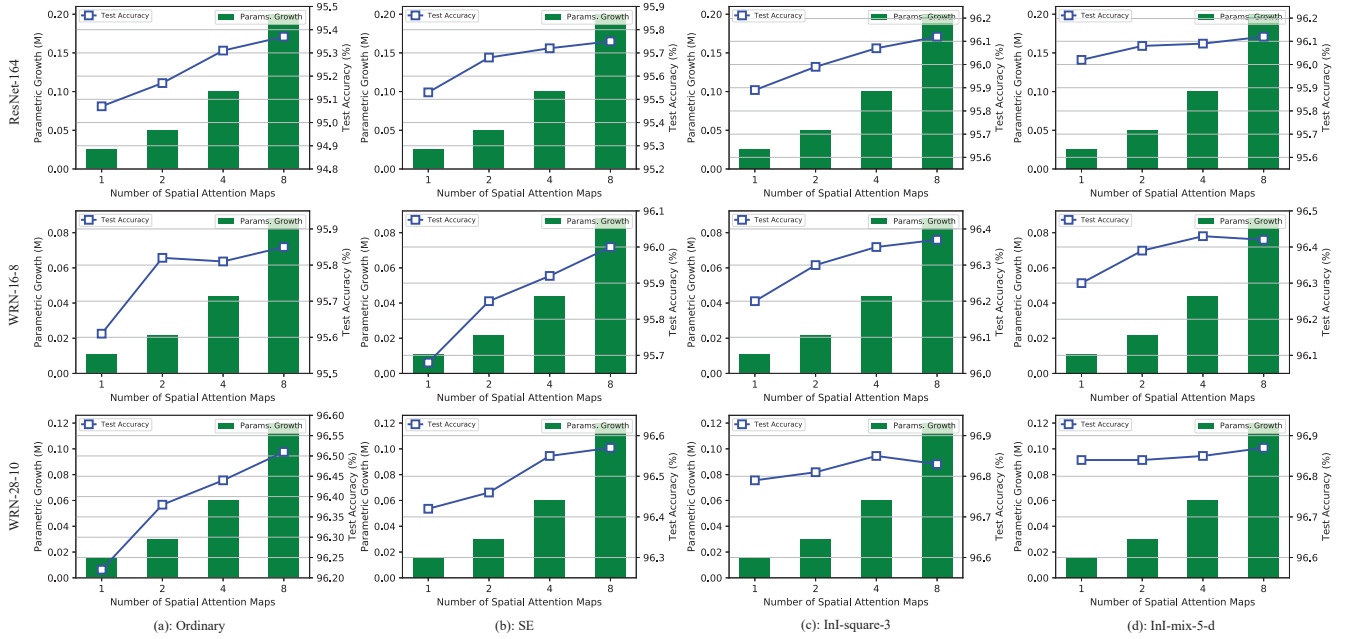


Fig. 9: The amount of parameter growth and test accuracy concerning the number of spatial attention maps with various networks under modes of (a): ordinary; (b) SE; (c) InI-square-3 and (d) InI-mix-5-d on CIFAR-10.

TABLE V: Test error((mean \pm std) %) of InI-models over 5 runs, compare with state-of-the-art results, using pre-act ResNet, WRN and PyramidNet as backbone, on CIFAR and SVHN. The top-three results are **red**, **green** and **blue** respectively.

Model	Depth	Params.	CIFAR-10	CIFAR-100	SVHN
original ResNet [10]	110	1.7M	6.43	25.16	–
pre-act ResNet [66]	164	1.7M	5.46	24.33	–
	1001	10.2M	4.62	22.71	–
ResNet Stochastic depth [35]	110	1.7M	5.23	24.58	1.75
	1202	10.2M	4.91	–	–
Wide ResNet [34]	28	36.5M	4.17	20.50	–
FractalNet [15]	21	38.6M	5.22	23.30	2.01
W/dropout & droppath	21	38.6M	4.60	23.73	1.87
DenseNet [47]	100	27.2M	3.74	19.25	1.59
DenseNet-BC ($k = 40$)	190	25.6M	3.46	17.18	–
ResNeXt [74]	29	34.4M	3.65	17.77	–
PyramidNet [71]	272	26.0M	3.31	16.35	–
CliqueNet ($k = 80/k = 150$) [48]	15	8M	5.17	22.78	1.53
	30	10M	5.06	21.83	1.64
DMRNet-Wide [45]	32	14.9M	3.94	19.25	1.51
DMRNet-Wide [45]	50	24.8M	3.57	19.00	1.55
DMRNeXt [45]	29	26.7M	3.06	17.55	–
InI-ResNet-simple-3 (ours)	164	2.02M	4.32	21.63	–
InI-ResNet-square-3 (ours)	164	2.02M	4.22	21.52	–
InI-WRN-simple-3 (ours)	28	36.85M	3.35	18.27	–
InI-WRN-square-3 (ours)	28	36.88M	3.29	18.11	1.49
InI-WRN-mix-5 (ours)	28	36.90M	3.25	18.03	1.53
InI-WRN-mix-5-d (ours)	28	36.90M	3.22	17.96	1.47
InI-PyramidNet-square-3 (ours)	272	27.5M	3.13	15.97	–
InI-PyramidNet-mix-5 (ours)	272	27.8M	3.09	15.83	–
InI-PyramidNet-mix-5-d (ours)	272	27.8M	3.07	15.78	–

that the InI model needs to rely on many hyper-parametric adjustments. On the contrary, the InI model is insensitive to hyper-parameters such as the G-filter type. Conventional G-filter selection and the simple combination can obtain very competitive performance, illustrating that InI model is very robust. At the same time, the InI model is highly scalable and flexible. The various patterns and combinations of the InI model can be extended to pursue extreme excelsior modeling performance.

The InI model has high universality, so that it can be applied to any CNN structure. It also has good adaptability to other enhancement mechanisms for CNNs, such as spatial attention.

VI. CONCLUSION

In this paper, we propose the Inner-Imaging architecture for convolutional networks, which present a novel strategy to model the channel relationships in CNNs. The proposed Inner-Imaging architecture uses the convolutional G-filter to organize

TABLE VI: Single crop error rates (%) on ImageNet.

Model	Params.	top-1	top-5
ResNet-50 [10]	25.60M	24.70	7.80
ResNet-101 [10]	44.60M	23.60	7.10
ResNet-152 [10]	60.30M	23.00	6.7
DenseNet-121 [47]	7.98M	25.02	7.71
CliqueNet [48]	14.38M	24.01	7.15
SE-ResNet-50 [21]	28.10M	23.29	6.62
SE-ResNet-101 [21]	49.40M	22.38	6.07
SE-ResNet-152 [21]	65.50M	21.57	5.73
InI-ResNet-50-mix-5-d (ours)	28.77M	22.08	5.76
InI-ResNet-101-mix-5-d (ours)	50.58M	21.34	5.27
CBAM-ResNet-50 [30]	28.16M	22.66	6.31
CBAM-ResNet-101 [30]	49.48M	21.51	5.69
InI-ResNet-50-mix-5-d + spa (ours)	28.83M	21.41	5.55
InI-ResNet-50-mix-5-d + spa \times 4 (ours)	50.66M	21.17	5.42
InI-ResNet-101-mix-5-d + spa (ours)	29.00M	20.80	5.16
InI-ResNet-101-mix-5-d + spa \times 4 (ours)	50.89M	20.54	5.07

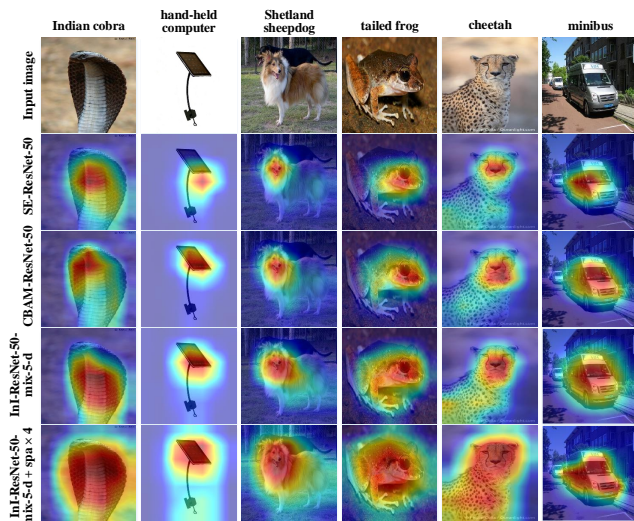


Fig. 10: The Grad-CAM [75] visualization for different models with the backbone of ResNet-50, on ImageNet.

the grouping relations of the channels, explicitly models the channel in-group coordination and the inter-group complementary relations. This design effectively improves the modeling efficiency of convolutional networks. The proposed method is easy to use and extensible, and its superior performance is verified on multiple benchmark datasets.

ACKNOWLEDGMENT

This study was supported by China National Science Foundation (Grant Nos. 60973083 and 61273363), Science and Technology Planning Project of Guangdong Province (Grant Nos. 2014A010103009 and 2015A020217002), Guangzhou Science and Technology Planning Project (Grant Nos. 201604020179, 201803010088), Guangdong Province Higher Vocational Colleges and Schools Pearl River Scholar Funded Scheme under Grant 2018, China National Natural Science Foundation (Grant Nos. 61722205, 61751205, 61751202, 61572199, 61502174, and U1611461), Science and Technology Planning Projects of Guangdong Province (Grant No. 2018B010107002).

REFERENCES

- [1] C. Szegedy, W. Liu, Y. Jia, P. Sermanet, S. E. Reed, D. Anguelov, D. Erhan, V. Vanhoucke, and A. Rabinovich, "Going deeper with convolutions," *computer vision and pattern recognition*, pp. 1–9, 2015.
- [2] K. Simonyan and A. Zisserman, "Very deep convolutional networks for large-scale image recognition," *international conference on learning representations*, 2015.
- [3] Y. Wei, Y. Zhao, C. Lu, S. Wei, L. Liu, Z. Zhu, and S. Yan, "Cross-modal retrieval with cnn visual features: A new baseline," *IEEE transactions on cybernetics*, vol. 47, no. 2, pp. 449–460, 2017.
- [4] L. Wu, J.-Z. Cheng, S. Li, B. Lei, T. Wang, and D. Ni, "Fuika: Fetal ultrasound image quality assessment with deep convolutional networks," *IEEE transactions on cybernetics*, vol. 47, no. 5, pp. 1336–1349, 2017.
- [5] W. Wu, Y. Yin, X. Wang, and D. Xu, "Face detection with different scales based on faster r-cnn," *IEEE transactions on cybernetics*, no. 99, pp. 1–12, 2018.
- [6] X. Li, Y. Zhang, Q. Cui, X. Yi, and Y. Zhang, "Tooth-marked tongue recognition using multiple instance learning and cnn features," *IEEE transactions on cybernetics*, no. 99, pp. 1–8, 2018.
- [7] Y. Hu, G. Wen, H. Liao, C. Wang, D. Dai, and Z. Yu, "Automatic construction of chinese herbal prescriptions from tongue images using cnns and auxiliary latent therapy topics," *IEEE transactions on cybernetics*, 2019.
- [8] J. Gu, Z. Wang, J. Kuen, L. Ma, A. Shahroudy, B. Shuai, T. Liu, X. Wang, G. Wang, J. Cai *et al.*, "Recent advances in convolutional neural networks," *Pattern Recognition*, vol. 77, pp. 354–377, 2018.
- [9] K. He, X. Zhang, S. Ren, and J. Sun, "Spatial pyramid pooling in deep convolutional networks for visual recognition," *IEEE Transactions on Pattern Analysis and Machine Intelligence*, vol. 37, no. 9, pp. 1904–1916, 2015.
- [10] —, "Deep residual learning for image recognition," *computer vision and pattern recognition*, pp. 770–778, 2016.
- [11] M. Zhang, W. Li, Q. Du, L. Gao, and B. Zhang, "Feature extraction for classification of hyperspectral and lidar data using patch-to-patch cnn," *IEEE transactions on cybernetics*, 2018.
- [12] H. Wang, P. Chen, and S. Kwong, "Building correlations between filters in convolutional neural networks," *IEEE transactions on cybernetics*, vol. 47, no. 10, pp. 3218–3229, 2017.
- [13] L. Wang, X. Qian, Y. Zhang, J. Shen, and X. Cao, "Enhancing sketch-based image retrieval by cnn semantic re-ranking," *IEEE transactions on cybernetics*, pp. 1–13, 2019.
- [14] X. Zhang, Z. Li, C. Change Loy, and D. Lin, "Polynet: A pursuit of structural diversity in very deep networks," in *computer vision and pattern recognition*, 2017, pp. 718–726.
- [15] G. Larsson, M. Maire, and G. Shakhnarovich, "Fractalnet: Ultra-deep neural networks without residuals," *international conference on learning representations*, 2017.
- [16] R. Yu, A. Li, C. Chen, J. Lai, V. I. Morariu, X. Han, M. Gao, C. Lin, and L. S. Davis, "Nisp: Pruning networks using neuron importance score propagation," *computer vision and pattern recognition*, pp. 9194–9203, 2018.
- [17] G. Zhu, J. Wang, P. Wang, Y. Wu, and H. Lu, "Feature distilled tracking," *IEEE transactions on cybernetics*, no. 99, pp. 1–13, 2017.
- [18] L. Zeng and X. Tian, "Accelerating convolutional neural networks by removing interspatial and interkernel redundancies," *IEEE transactions on cybernetics*, 2018.
- [19] M. Sandler, A. Howard, M. Zhu, A. Zhmoginov, and L.-C. Chen, "Mobilenetv2: Inverted residuals and linear bottlenecks," in *computer vision and pattern recognition*, 2018, pp. 4510–4520.
- [20] N. Ma, X. Zhang, H.-T. Zheng, and J. Sun, "Shufflenet v2: Practical guidelines for efficient cnn architecture design," in *europa conference on computer vision*, 2018, pp. 116–131.
- [21] J. Hu, L. Shen, and G. Sun, "Squeeze-and-excitation networks," *computer vision and pattern recognition*, 2018.
- [22] F. Chollet, "Xception: Deep learning with depthwise separable convolutions," in *computer vision and pattern recognition*, 2017, pp. 1251–1258.
- [23] X. Zhang, X. Zhou, M. Lin, and J. Sun, "Shufflenet: An extremely efficient convolutional neural network for mobile devices," in *computer vision and pattern recognition*, 2018, pp. 6848–6856.
- [24] G. Huang, S. Liu, L. Van der Maaten, and K. Q. Weinberger, "Condensnet: An efficient densenet using learned group convolutions," in *computer vision and pattern recognition*, 2018, pp. 2752–2761.
- [25] X. Chen, J. Weng, W. Lu, J. Xu, and J. Weng, "Deep manifold learning combined with convolutional neural networks for action recognition," *IEEE Transactions on Neural Networks and Learning Systems*, vol. PP, no. 99, pp. 1–15, 2018.

- [26] Z. Liao and G. Carneiro, "A deep convolutional neural network module that promotes competition of multiple-size filters," *Pattern Recognition*, vol. 71, pp. 94–105, 2017.
- [27] B. Zoph, V. Vasudevan, J. Shlens, and Q. V. Le, "Learning transferable architectures for scalable image recognition," *computer vision and pattern recognition*, 2018.
- [28] H. Pham, M. Y. Guan, B. Zoph, Q. V. Le, and J. Dean, "Efficient neural architecture search via parameters sharing," *international conference on machine learning*, pp. 4092–4101, 2018.
- [29] L. Chen, H. Zhang, J. Xiao, L. Nie, J. Shao, W. Liu, and T. Chua, "Sca-cnn: Spatial and channel-wise attention in convolutional networks for image captioning," *computer vision and pattern recognition*, pp. 6298–6306, 2017.
- [30] S. Woo, J. Park, J. Lee, and I. S. Kweon, "Cbam: Convolutional block attention module," *eupean conference on computer vision*, pp. 3–19, 2018.
- [31] J. Cheng, J. Wu, C. Leng, Y. Wang, and Q. Hu, "Quantized cnn: a unified approach to accelerate and compress convolutional networks," *IEEE transactions on neural networks and learning systems*, no. 99, pp. 1–14, 2017.
- [32] F. Yu, D. Wang, E. Shelhamer, and T. Darrell, "Deep layer aggregation," in *computer vision and pattern recognition*, 2018, pp. 2403–2412.
- [33] F. Tung and G. Mori, "Deep neural network compression by in-parallel pruning-quantization," *IEEE transactions on pattern analysis and machine intelligence*, 2018.
- [34] S. Zagoruyko and N. Komodakis, "Wide residual networks," pp. 87.1–87.12, 2016.
- [35] G. Huang, Y. Sun, Z. Liu, D. Sedra, and K. Q. Weinberger, "Deep networks with stochastic depth," *eupean conference on computer vision*, pp. 646–661, 2016.
- [36] A. Veit, M. J. Wilber, and S. J. Belongie, "Residual networks behave like ensembles of relatively shallow networks," *neural information processing systems*, pp. 550–558, 2016.
- [37] Y. Lu, G. Lu, Y. Xu, and B. Zhang, "Aar-cnns: Auto adaptive regularized convolutional neural networks," *international joint conference on artificial intelligence*, pp. 2511–2517, 2018.
- [38] S. Lin, R. Ji, Y. Li, C. Deng, and X. Li, "Towards compact convnets via structure-sparsity regularized filter pruning," *IEEE transactions on neural networks and learning systems*, 2019.
- [39] M. Wang, C. Luo, R. Hong, J. Tang, and J. Feng, "Beyond object proposals: Random crop pooling for multi-label image recognition," *IEEE Transactions on Image Processing*, vol. 25, no. 12, pp. 5678–5688, 2016.
- [40] G. Ghiasi, T.-Y. Lin, and Q. V. Le, "Dropblock: A regularization method for convolutional networks," in *Advances in Neural Information Processing Systems*, 2018, pp. 10727–10737.
- [41] Z. Wu, T. Nagarajan, A. Kumar, S. J. Rennie, L. S. Davis, K. Grauman, and R. S. Feris, "Blockdrop: Dynamic inference paths in residual networks," *computer vision and pattern recognition*, pp. 8817–8826, 2018.
- [42] C. Liu, T. Lin, Y. Wu, Y. Lin, H. Lee, Y. Tsao, and S. Chien, "Computation-performance optimization of convolutional neural networks with redundant filter removal," *IEEE Transactions on Circuits and Systems I-regular Papers*, pp. 1–14, 2018.
- [43] J. Luo, H. Zhang, H. Zhou, C. Xie, J. Wu, and W. Lin, "Thinet: Pruning cnn filters for a thinner net," *IEEE Transactions on Pattern Analysis and Machine Intelligence*, pp. 1–1, 2018.
- [44] M. Figurov, M. D. Collins, Y. Zhu, L. Zhang, J. Huang, D. P. Vetrov, and R. Salakhutdinov, "Spatially adaptive computation time for residual networks," *computer vision and pattern recognition*, pp. 1790–1799, 2017.
- [45] L. Zhao, M. Li, D. Meng, X. Li, Z. Zhang, Y. Zhuang, Z. Tu, and J. Wang, "Deep convolutional neural networks with merge-and-run mappings," *international joint conference on artificial intelligence*, pp. 3170–3176, 2018.
- [46] Z. Huo, B. Gu, and H. Huang, "Training neural networks using features replay," *neural information processing systems*, pp. 6660–6669, 2018.
- [47] G. Huang, Z. Liu, L. V. Der Maaten, and K. Q. Weinberger, "Densely connected convolutional networks," *computer vision and pattern recognition*, pp. 2261–2269, 2017.
- [48] Y. Yang, Z. Zhong, T. Shen, and Z. Lin, "Convolutional neural networks with alternately updated clique," *computer vision and pattern recognition*, pp. 2413–2422, 2018.
- [49] J. Adebayo, J. Gilmer, M. C. Muelly, I. J. Goodfellow, M. Hardt, and B. Kim, "Sanity checks for saliency maps," *neural information processing systems*, pp. 9505–9515, 2018.
- [50] H. Gao, Z. Wang, and S. Ji, "Channelnets: Compact and efficient convolutional neural networks via channel-wise convolutions," *neural information processing systems*, pp. 5197–5205, 2018.
- [51] T. V. Nguyen, Q. Zhao, and S. Yan, "Attentive systems: A survey," *International Journal of Computer Vision*, vol. 126, no. 1, pp. 86–110, 2018.
- [52] W. Li, X. Zhu, and S. Gong, "Harmonious attention network for person re-identification," *computer vision and pattern recognition*, pp. 2285–2294, 2018.
- [53] W. Li, F. Abtahi, Z. Zhu, and L. Yin, "Eac-net: Deep nets with enhancing and cropping for facial action unit detection," *IEEE Transactions on Pattern Analysis and Machine Intelligence*, pp. 1–1, 2018.
- [54] Y. Li, X. Wang, W. Liu, and B. Feng, "Deep attention network for joint hand gesture localization and recognition using static rgb-d images," *Information Sciences*, vol. 441, pp. 66–78, 2018.
- [55] X. Zhang, Y. Su, Z. He, X. Liu, and J. Wu, "Medical exam question answering with large-scale reading comprehension," *national conference on artificial intelligence*, pp. 5706–5713, 2018.
- [56] J. Hou, X. Wu, Y. Sun, and Y. Jia, "Content-attention representation by factorized action-scene network for action recognition," *IEEE Transactions on Multimedia*, vol. 20, no. 6, pp. 1537–1547, 2018.
- [57] L. Chen, Y. Yang, J. Wang, W. Xu, and A. L. Yuille, "Attention to scale: Scale-aware semantic image segmentation," *computer vision and pattern recognition*, pp. 3640–3649, 2016.
- [58] A. Newell, K. Yang, and J. Deng, "Stacked hourglass networks for human pose estimation," *eupean conference on computer vision*, pp. 483–499, 2016.
- [59] M. Jaderberg, K. Simonyan, A. Zisserman, and K. Kavukcuoglu, "Spatial transformer networks," *neural information processing systems*, pp. 2017–2025, 2015.
- [60] H. Tang, B. Xiao, W. Li, and G. Wang, "Pixel convolutional neural network for multi-focus image fusion," *Information Sciences*, pp. 125–141, 2017.
- [61] E. Perez, F. Strub, H. De Vries, V. Dumoulin, and A. C. Courville, "Film: Visual reasoning with a general conditioning layer," *national conference on artificial intelligence*, pp. 3942–3951, 2018.
- [62] M. F. Stollenga, J. Masci, F. J. Gomez, and J. Schmidhuber, "Deep networks with internal selective attention through feedback connections," *neural information processing systems*, pp. 3545–3553, 2014.
- [63] X. Zhang, X. Zhou, M. Lin, and J. Sun, "Shufflenet: An extremely efficient convolutional neural network for mobile devices," *computer vision and pattern recognition*, pp. 6848–6856, 2018.
- [64] X. Wang, Y. Yan, P. Tang, X. Bai, and W. Liu, "Revisiting multiple instance neural networks," *Pattern Recognition*, vol. 74, pp. 15–24, 2018.
- [65] J. Hu, L. Shen, S. Albanie, G. Sun, and A. Vedaldi, "Gather-excite: Exploiting feature context in convolutional neural networks," *neural information processing systems*, pp. 9401–9411, 2018.
- [66] K. He, X. Zhang, S. Ren, and J. Sun, "Identity mappings in deep residual networks," *eupean conference on computer vision*, pp. 630–645, 2016.
- [67] A. Krizhevsky and G. Hinton, "Learning multiple layers of features from tiny images," *handbook of hystemic autoimmune diseases*, vol. 1, no. 4, 2009.
- [68] Y. Netzer, T. Wang, A. Coates, A. Bissacco, B. Wu, and A. Y. Ng, "Reading digits in natural images with unsupervised feature learning," *nips workshop on deep learning & unsupervised feature learning*, 2012.
- [69] J. Deng, W. Dong, R. Socher, L. Li, K. Li, and L. Feifei, "Imagenet: A large-scale hierarchical image database," *computer vision and pattern recognition*, pp. 248–255, 2009.
- [70] J. Springenberg, A. Dosovitskiy, T. Brox, and M. Riedmiller, "Striving for simplicity: The all convolutional net," *international conference on learning representations (workshop track)*, 2014.
- [71] D. Han, J. Kim, and J. Kim, "Deep pyramidal residual networks," *computer vision and pattern recognition*, pp. 6307–6315, 2017.
- [72] S. Ioffe and C. Szegedy, "Batch normalization: Accelerating deep network training by reducing internal covariate shift," *International Conference on Machine Learning*, pp. 448–456, 2015.
- [73] F. Yu and V. Koltun, "Multi-scale context aggregation by dilated convolutions," *international conference on learning representations*, 2016.
- [74] S. Xie, R. B. Girshick, P. Dollár, Z. Tu, and K. He, "Aggregated residual transformations for deep neural networks," *computer vision and pattern recognition*, pp. 5987–5995, 2017.
- [75] R. R. Selvaraju, M. Cogswell, A. Das, R. Vedantam, D. Parikh, and D. Batra, "Grad-cam: Visual explanations from deep networks via gradient-based localization," *international conference on computer vision*, pp. 618–626, 2017.